# High-Strength Low-Carbon Ferritic Steel Containing Cu-Fe-Ni-Al-Mn Precipitates

SEMYON VAYNMAN, DIETER ISHEIM, R. PRAKASH KOLLI, SHRIKANT P. BHAT, DAVID N. SEIDMAN, and MORRIS E. FINE

An investigation of a low-carbon, Fe-Cu–based steel, for Naval ship hull applications, with a yield strength of 965 MPa, Charpy V-notch absorbed impact-energy values as high as 74 J at –40 °C, and an elongation-to-failure greater than 15 pct, is presented. The increase in strength is derived from a large number density (approximately $10^{23}$ to $10^{24}$ $m^{-3}$) of copper-iron-nickel-aluminum-manganese precipitates. The effect on the mechanical properties of varying the thermal treatment was studied. The nanostructure of the precipitates found within the steel was characterized by atom-probe tomography. Additionally, initial welding studies show that a brittle heat-affected zone is not formed adjacent to the welds.

DOI: 10.1007/s11661-007-9417-x


## I. INTRODUCTION

APPROXIMATELY 20 years ago, the United States Navy developed a high-strength low-alloy (HSLA) steel, denoted HSLA-100, with a yield strength of 100 ksi (689 MPa), as a replacement for HY-100 steel to reduce fabrication costs in ship construction.[1–4] HSLA-100 possesses similar strength and toughness values as HY-100, but because of the reduced nominal carbon content, it is weldable without preheat, thereby reducing fabrication costs.[3–5] To compensate for the decrease in strength on reducing the C concentration, Cu was added to HSLA-100 for precipitation strengthening, whereas Cr, Ni, and Mo were added to increase hardenability.[2–7]

The thermal processing of HSLA-100, a solutionizing (austenitizing) and quenching step followed by tempering at 620 °C to 690 °C, produced a tempered martensitic steel containing Cu precipitates.[2–4] Studies by Foley *et al.*[8,9] have demonstrated that tempering of HSLA-100 overages the Cu precipitates, thereby reducing their strengthening contribution.

Earlier research on steels alloyed with Cu, however, showed that significant strengthening could be attained without tempering.[10–13] To develop a precipitation-strengthened ferritic variant of HSLA-100 steel, Mo and Cr were removed, reducing hardenability, and the thermal processing was simplified to hot rolling followed by air cooling. These changes produced a ferritic HSLA plate steel with a yield strength in excess of 482 MPa (70 ksi), a Charpy V-notch (CVN) absorbed impact-energy better than 136 J (100 ft-lbs) at –40 °C, improved weldability, and enhanced atmospheric corrosion resistance.[8,14–18] This steel, ASTM A710 grade B, was used in construction of a demonstration bridge in northern Illinois. The body-centered-cubic (bcc) nanoscale Cu precipitates within the steel are coherent with the matrix providing significant precipitation strengthening. Goodman *et al.* first documented this in a binary Fe-Cu steel many years ago by using field-ion and atom-probe microscopies.[19,20]

Additional increases in yield strength were achieved by changing the thermal processing to hot rolling followed by quenching into water and subsequently isothermal aging. The result was a high-strength low-carbon (HSLC) steel with yield strengths of approximately 700 MPa (100 ksi) and excellent CVN absorbed impact-energy values.[18,21] This steel is denoted NUCu-100, where the number 100 stands for the yield strength of the steel in ksi.* For example, when NUCu-100 is solutionized at 900 °C and aged at 524 °C, the steel achieves a yield strength of 712 MPa (103 ksi) at room temperature and a CVN absorbed impact energy of 64 J (47 ft-lbs) at –40 °C.[18] The strength of this steel is derived primarily from bcc Cu precipitates, although there is possibly a small contribution from niobium-carbide (NbC) precipitates at long aging times that delays overaging.[21–23]

Investigation, by atom-probe tomography (APT)[24–26] of the bcc Cu precipitates in a NUCu-100 steel specimen solutionized for 30 minutes at 1100 °C and directly aged for 100 minutes at 490 °C demonstrated the existence of chemically complex Cu-rich precipitates containing Fe, Ni, Mn, and Al.[27,28] The precipitate/α-Fe matrix

*The term NUCu stands for Northwestern University copper alloyed steel.

SEMYON VAYNMAN, Research Professor and MORRIS E. FINE, Professor, Member of Graduate Faculty, Department of Materials Science and Engineering, and DIETER ISHEIM, Research Assistant Professor, and DAVID N. SEIDMAN, W.P. Murphy Professor, Department of Materials Science and Engineering and Northwestern University Center for Atom-Probe Tomography (NUCAPT), are with Northwestern University Evanston, IL 60208-3108. Contact email: svaynman@northwestern.edu R. PRAKASH KOLLI, Senior Metallurgist, is with Global Customer Analytical, Nalco Company, Naperville, IL 60563 and SHRIKANT P. BHAT, Manager, is with ArcelorMittal Steel Global Research & Development, East Chicago, IN 46312.

Manuscript submitted May 11, 2007.
Article published online January 9, 2008

heterophase interfaces are enriched in Ni and Mn forming a spherical shell-like structure, whereas the Al enhancement is found toward the inner region of the Cu precipitates.

The focus of the present study is investigation of a ferritic multicomponent Fe-Cu–based steel with a yield strength of 965 MPa (140 ksi), which also possesses an elongation-to-failure greater than 15 pct, a CVN absorbed impact-energy as high as 74 J at –40 °C, potentially improved weldability (no brittle heat-affected zone), and better corrosion resistance. This HSLC steel is being studied in a program to develop an explosion resistant steel[29] for the United States Navy.

We first discuss the results of preliminary research on an arc-melted heat demonstrating the viability of developing a HSLC steel with the described properties. We then discuss the results of a more comprehensive investigation on three 45.5-kg (100-lb) laboratory heats processed by ArcelorMittal Steel Global Research & Development Laboratory. We show the effects on microstructure and mechanical properties of increasing the nominal Ni and Al concentrations from that found in NUCu-100. The presence of the Cu-rich[30] precipitates is verified and characterized in detail using APT. Additionally, NbC and heterogeneously nucleated NiAl-type precipitates are present. The results of preliminary welding studies are discussed.

## II. PRELIMINARY RESEARCH

Initial research was done on a 100-gram steel heat arc-melted in an argon atmosphere. Additional Ni and Al (> 99.99 at. pct pure) were added to a piece of 525 MPa (76 ksi) yield strength NUCu steel. Ni and Al have an additive effect on the precipitation strengthening,[31–33] permitting the development of even stronger steels. The Ni and Al concentrations were selected based on prior experience.[34,35] The composition of the arc-melted steel heat is given in Table I. The resulting 12.3-mm-diameter ingot was homogenized at 1150 °C for 72 hours and then cold swaged, without intermediate anneals, producing a 6-mm-diameter rod. This represents a 75 pct reduction in area, indicating that this steel possesses a significant capacity for cold working. The rods were solutionized at 1050 °C, quenched into water at room temperature, and subsequently aged at 550 °C for 2 hours. Subsized tensile specimens with a 25.4-mm (1-in.) gage length were machined from the rod.

Tensile tests were performed at room temperature and at –35 °C. At both temperatures, yield strengths of approximately 840 MPa (122 ksi) and ultimate tensile strengths of approximately 945 MPa (137 ksi) were obtained. The elongation-to-failure was approximately 30 pct at both testing temperatures. The fracture was completely ductile as characterized by the fracture surface. Additionally, a subscale CVN specimen tested at –35 °C only partially fractured and bent in the testing apparatus. As with the tensile specimens, the fracture was ductile.

## III. EXPERIMENTAL METHODS

### A. *Alloy Details*

Three 45.5-kg (100-lb) laboratory heats were produced for this research at ArcelorMittal Steel Global Research & Development Laboratory by vacuum induction melting. The resulting slabs were prepared (top cropped, and the sides machined) and reheated to approximately 1150 °C and hot rolled into 12.3-mm-(0.5-in.-) thick plates in several passes. The temperature of the final pass was approximately 900 °C. The compositions of the three heats, determined by spectrographic analysis at ArcelorMittal Steel, are given in Table I. The heats are denoted NUCu-140-*x*, where 140 stands for the target yield strength in ksi and *x* designates the heat number.** The *N* content does not exceed 0.001 wt pct, a result of the vacuum induction melting process. The nominal concentrations of *S* and *P* should be as small as possible. In the NUCu-140-2 heat, however, the *P* concentration is 0.014 wt pct, which is 2 to 4 times greater than in the other two heats. The plates were mechanically cut into rods (12.3 mm × 12.3 mm × 250 mm) and solutionized at 900 °C, 1000 °C, or 1100 °C, followed by quenching into water at room temperature.

**In earlier publications and conference proceedings, we denoted the same heats as NUCu-150-*x* or AlNiCu-150-*x*. We make the change to NUCu-140-*x* to better relate the steel to similar Cu alloyed steels previously developed at Northwestern University.

**Table I. Compositions of NUCu-140-*x* Steels (Weight Percent and Atomic Percent)***

| | | C | Mn | Si | Cu | Ni | Al | Nb | P | S |
|---|---|---|---|---|---|---|---|---|---|---|
| Arc-melted steel | wt pct | 0.04 | 0.47 | 0.47 | 1.36 | 2.78 | 0.66 | 0.07 | 0.007 | 0.001 |
| | at. pct | 0.19 | 0.48 | 0.94 | 1.19 | 2.64 | 1.37 | 0.042 | 0.013 | 0.002 |
| NUCu-140-1 | wt pct | 0.05 | 0.47 | 0.46 | 1.34 | 2.71 | 0.60 | 0.07 | 0.005 | 0.001 |
| | at. pct | 0.23 | 0.48 | 0.92 | 1.17 | 2.57 | 1.24 | 0.042 | 0.009 | 0.002 |
| NUCu-140-2 | wt pct | 0.04 | 0.48 | 0.48 | 1.37 | 2.86 | 0.69 | 0.07 | 0.014 | 0.004 |
| | at. pct | 0.19 | 0.49 | 0.96 | 1.20 | 2.71 | 1.43 | 0.042 | 0.025 | 0.007 |
| NUCu-140-3 | wt pct | 0.05 | 0.52 | 0.48 | 1.29 | 2.87 | 0.58 | 0.07 | 0.004 | 0.005 |
| | at. pct | 0.23 | 0.53 | 0.96 | 1.13 | 2.72 | 1.20 | 0.042 | 0.007 | 0.009 |

*Nitrogen content does not exceed 0.001 wt pct.

The tensile specimens are ASTM standard specimens (ASTM E 8 – 04) with a gage length of 25.4-mm (1-in.) and a diameter of 6-mm (0.25-in.). The CVN specimens are also ASTM standard size specimens (ASTM E 23 – 02a). The specimens and additional material (12.3 mm × 12.3 mm × 25 mm blocks) for hardness testing and APT were solutionized at 900° C and aged either at 500 °C or 550 °C and then quenched into water at room temperature precluding extra precipitation. The hardness and APT specimens were aged from 1 to 100 hours, whereas the tensile and CVN specimens were aged either for 6 hours at 500 °C or 2 hours at 550 °C.

### B. *Optical Microscopy*

Sections of the solutionized and water-quenched specimens perpendicular to the rolling direction were cold mounted and polished to a final surface finish of 1 $\mu$m using standard procedures. The mounted specimens were etched for approximately 10 to 15 seconds with a 2 vol pct Nital solution allowing observation of the microstructures.

### C. *Mechanical Properties*

Hardness testing was performed using a Wilson Rockwell hardness tester using the standard Rockwell diamond indenter and a 150-kg testing load (Rockwell C scale). Tensile testing was performed on a Sintech screw-driven testing machine in accordance with ASTM standards (ASTM E 8 – 04), with a 20-kilopound (kip) load cell under displacement control at a strain rate of 0.04 $s^{-1}$. The specimen strain was measured using a 1-in. extensometer. The CVN tests were performed using a Tinius Olsen impact-testing machine in accordance with ASTM standards (ASTM E 23 – 02a).

### D. *Welding Studies*

Welding tests were performed on the NUCu-140-1 steel heat. Welding rods for the 965 MPa yield strength level are not commercially available; therefore, a 10-mm-diameter section of NUCu-140-1 steel was cold swaged to a 2.5-mm diameter for use as a welding rod. A 12.3-mm-thick plate of NUCu-140-1 was solutionized at 900 °C, water quenched to room temperature, and then aged for 2 hours at 550 °C. A bead of the welding rod was melted on the aged plate using argon-shielded metal arc welding; the heat input was 3.6 kJ $mm^{-1}$ and the travel speed was 2.5 mm $s^{-1}$.

Specimens were mechanically cut from the welded plate, cold mounted, and polished, using standard procedures, to a final surface finish of 1 $\mu$m for optical microscopy and hardness testing. Hardness testing was performed in accordance with ASTM standards (ASTM E 384 – 99) using a Buehler Micromet II microhardness tester with a Vickers microhardness indenter, a load of 200 g, and a testing time of 10 seconds. The results were reported in GPa. Vickers microhardness (HVN) testing was performed to discern the changes in hardness within the weld, fusion zone (FZ), and heat-affected zone (HAZ) on a shorter length scale than accessible with standard Rockwell hardness C (HRC) testing. For optical microscopy, the specimens were etched for approximately 10 to 15 seconds with a 2 vol pct Nital solution.

### E. *Atom-Probe Tomography*

Atom-probe tomography tip blanks (0.3 mm × 0.3 mm × 25 mm) were mechanically cut from the aged blocks. The APT tip blanks were electropolished using standard procedures.[24,36] Initial polishing was performed with a solution of 10 vol pct perchloric acid in acetic acid at 8 to 20 Vdc at room temperature. This was followed by final electropolishing using a solution of 2 vol pct perchloric acid in butoxyethanol at 8 to 15 Vdc, producing a tip with a radius $< 50$ nm. LEAP and conventional three-dimensional atom-probe (3DAP) tomography[24–26] were performed at a specimen temperature of 50 K and a residual pressure of $< 1 \times 10^{-8}$ Pa. The pulse repetition rate was $2 \times 10^5$ Hz and the pulse-to-standing-dc voltage ratio (pulse fraction) was 15 to 20 pct. Visualization and quantitative evaluation of datasets were performed with the *Imago Visualization and Analysis Software (IVAS*[†]*)* and with ADAM 1.5, a custom software application developed at Northwestern University.[37] Compositional analyses of the precipitates, their heterophase interfaces, and matrix were performed with the proximity histogram method (proxigram for short), giving compositional profiles with respect to distance from an isoconcentration surface.[37–39] The Cu-rich precipitates were delineated by a 5 at. pct Cu isoconcentration surface. The parameters chosen for obtaining a noise-free reference isoconcentration surface are a voxel size of 0.8 to 1.0 nm, a delocalization distance of 2.0 nm, and a confidence sigma parameter ≤1. Neither the reference isoconcentration surface nor the proxigrams varied significantly when these parameters were changed by up to 50 pct, indicating a numerically stable evaluation procedure and representative results.

[†]IVAS is a trademark of Imago Scientific Instruments, Madison, WI.

The volume equivalent radius,[40] $R$, of a precipitate is given by

$$R = \left(\frac{3}{4\pi}\frac{n\Omega}{\eta}\right)^{\frac{1}{3}} \quad [1]$$

where $n$ is the number of atoms detected within a delineated precipitate, the atomic volume, $\Omega$, is $1.178 \times 10^{-2}$ $nm^3$ for bcc Fe, and the overall detection efficiency, $\eta$, of the multichannel detector plate is estimated to be 0.5. The value of $n$ belonging to a precipitate is determined from the envelope method[24,41] based on a maximum separation distance of 0.5 nm, a minimum precipitate size of 20 Cu atoms, and a grid spacing of 0.15 nm.

## IV. RESULTS

### A. *Optical Microscopy*

Figures 1(a) and 1(b) display the microstructure of NUCu-140-1 after quenching from 900 °C and 1100 °C, respectively. After quenching from 900 °C, the microstructure consists of equiaxed grains and a smaller volume fraction of elongated, acicular-like grains. The average ferrite grain size, determined by the ASTM intercept method (ASTM E 112 – 96), is 7 $\mu$m. Increasing the solutionizing temperature to 1100 °C increases significantly the average ferrite grain size to 42 $\mu$m and the grains are blocklike in shape with some containing distinct lathlike features. Solutionizing at 1000 °C gives an intermediate microstructure with a grain size of 24 $\mu$m. The ferrite grain size is controlled by temperature, time at temperature, and the presence of NbC in the austenite during solutionizing. The solubility of NbC in austenite increases as the temperature increases. For example, with low C content, the solubility of Nb in austenite increases from $3 \times 10^{-3}$ wt pct at 900 °C to $4 \times 10^{-2}$ wt pct at 1100 °C.[21–23]

The microstructure of NUCu-140-3 is similar to NUCu-140-1, but with a slightly larger grain size of 8.6 $\mu$m when solutionized at 900 °C. The grains of NUCu-140-2, when solutionized at 900 °C, are mixture of elongated acicular grains and blocklike grains, similar to that observed when NUCu-140-1 is solutionized at 1100 °C. The grain size is 10.3 $\mu$m.

### B. *Mechanical Properties*

Figure 2 shows hardness *vs* aging time for NUCu-140-1 as a function of solutionizing and aging temperatures. As depicted by the hardness curves the steel ages faster at an aging temperature of 550 °C than at 500 °C. Also, higher solutionizing temperatures result in an increased hardness. The measured maximum hardness at 500 °C (Figure 2(a)) aging is higher than that at 550 °C (Figure 2(b)). Two hardness peaks are observed at both aging temperatures. When aged at 500 °C, the first hardness peak occurs at 5 to 6 hours (Figure 2(a)), whereas the second peak occurs at approximately 12 to 24 hours (Figures 2(a) and 2(c)). At 100 hours, the hardness decreases to 37 from 38.5 HRC, indicating that the steel is overaged (Figure 2(c)). When aged at 550 °C, however, the first hardness peak occurs at approximately 2 hours, whereas the second peak occurs between 5 and 6 hours (Figure 2(b)). The hardness value decreases at 7 hours indicating overaging (Figure 2(c)).

Figure 3 shows the engineering stress *vs* engineering strain curves for NUCu-140-1 as a function of solution-

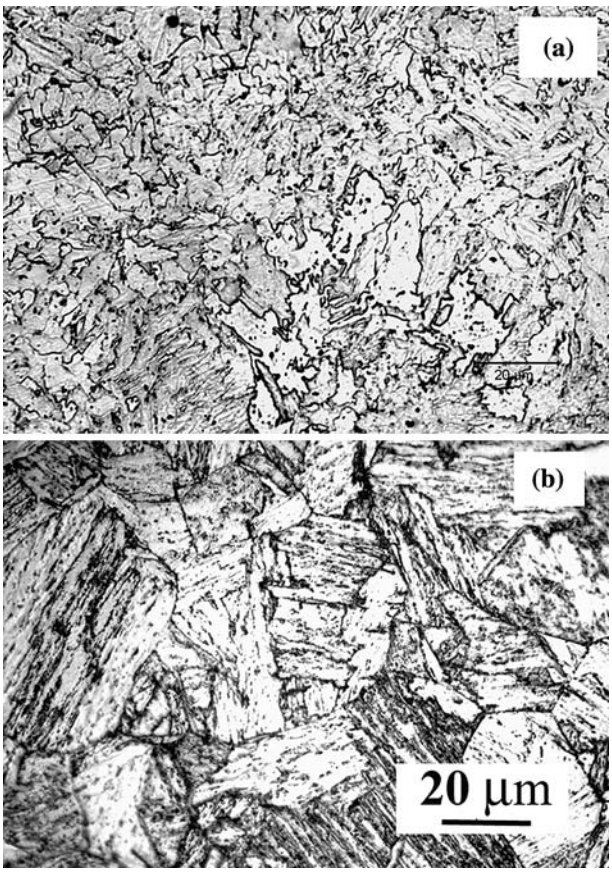


Fig. 1—Microstructure of NUCu-140-1 steel solutionized at (*a*) 900 °C or (*b*) 1100 °C and quenched into room-temperature water.

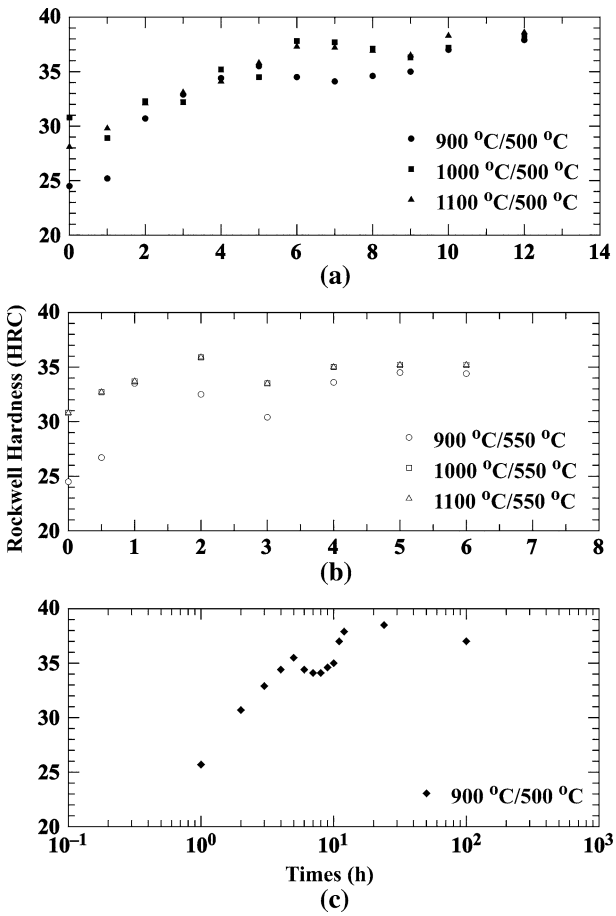


Fig. 2—Rockwell hardness C of NUCu-140-1 steel *vs* aging time, after solutionizing at 900 °C, when aged to (*a*) 12 h at 500 °C, to (*b*) 6 h at 550 °C, and to (*c*) 100 h at 500 °C.

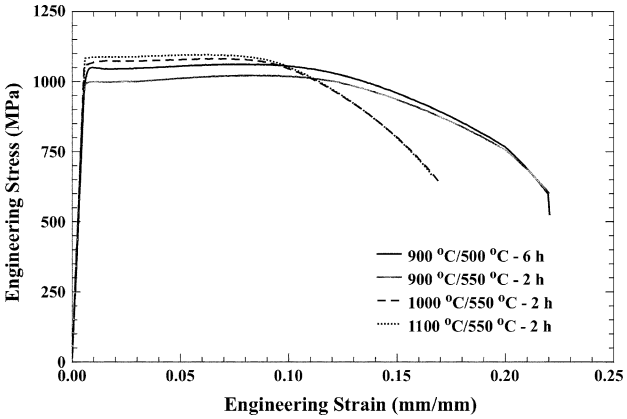


Fig. 3—Engineering stress *vs* engineering strain curves for NUCu-140-1 steel. The specimens are solutionized at 900 °C, 1000 °C, or 1100 °C and then aged for either 2 or 6 h at 500 °C or 550 °C. The strain rate is 0.04 $s^{-1}$.

izing and aging temperature. Increasing the solutionizing temperature results in greater yield and ultimate tensile strength values. The 0.2 pct offset yield strength of the steel after quenching from 900 °C and aging for 2 hours at 550 °C is 973 MPa (141 ksi). The yield strength increases by more than 10 pct to 1096 MPa (159 ksi) when the steel is quenched from 1100 °C and aged for 2 hours at 550 °C. This increase in yield strength, however, is accompanied by a decrease in elongation-to-failure from approximately 22 pct when solutionized at 900 °C to approximately 17 pct when the steel is solutionized at either 1000 °C or 1100 °C. NUCu-140-1 aged for 6 hours at 500 °C, however, has given a larger value of yield strength, 1001 MPa (145 ksi) than when aged at 550 °C for 2 hours. The tensile fracture surfaces of all the specimens exhibit a classic cup-and-cone type surface with dimpling indicating ductile failure.

Table II summarizes the tensile properties of the three steel heats when solutionized at 900 °C and aged for either 2 hours at 550 °C or 6 hours at 500 °C. A 900 °C solutionizing temperature was selected as this gives the most clearly ferritic microstructure (Figure 1) and the largest value for the elongation-to-failure, with only a minimal loss of yield strength when compared with solutionizing at 1000 °C or 1100 °C (Figure 3). The aging times were selected for near-peak hardness values at the given aging temperature (Figure 2).

When aged at 550 °C, NUCu-140-2 has the largest yield strength, 1049 MPa (152 ksi). The elongation-to-failure value is 20 pct, which is lower than the two other heats. NUCu-140-3 is the least strong heat with a yield strength of 849 MPa (123 ksi). Table III displays the CVN absorbed impact-energy values for the three heats when tested between 25 °C and –62 °C. NUCu-140-1 and NUCu-140-3 have similar values of CVN absorbed impact-energy and, therefore, possess good cryogenic impact toughness. NUCu-140-2, however, is more brittle at room temperature. Figures 4(a) and 4(b) display the fracture surfaces of NUCu-140-1 and NUCu-140-2 Charpy specimens tested at room temperature. The NUCu-140-1 specimen exhibits significant plastic deformation with shear lips seen on the edges and a granular center region. The NUCu-140-2 specimen shown exhibits little if any plastic deformation and the failure surface is cleavagelike, as determined by scanning electron microscopy (SEM).

When aged at 500 °C, NUCu-140-1 exhibits the largest value of the yield strength, 1001 MPa (145 ksi). NUCu-140-3 is somewhat weaker with a yield strength of 911 MPa (132 ksi). Both heats have similar values of elongation-to-failure, 22 pct. The CVN absorbed impact energies are significantly lower when the steel is aged at 500 °C. For example, when NUCu-140-1 is aged at 550 °C for 2 hours the absorbed impact-energy at room temperature is 208 J (153 ft-lbs), but when aged at 500 °C for 6 hours, the absorbed impact-energy at room temperature is only 82 J (60 ft-lbs). A comparable difference exists when the heat is tested at –23 °C. The NUCu-140-3 heat also demonstrates a similar variation when aged at 500 °C and 550 °C. We did not test NUCu-140-2 aged at 500 °C, because the CVN tests indicated that the heat is brittle under impact loading.

**Table III. Charpy V-Notch Absorbed Impact Energy for Steels Solutionized at 900 °C and Aged for 2 h at 550 °C**

| | Charpy Absorbed Impact Energy, J | | |
|---|---|---|---|
| Temperature, °C | NUCu-140-1 | NUCu-140-2 | NUCu-140-3 |
| 25 | 208 | 71 | 212 |
| –12 | 79 | — | — |
| –23 | 79 | 19 | 52 |
| –40 | 66 | — | 74 |
| –62 | 25 | — | — |

**Table II. Tensile Properties of NUCu-140-1, NUCu-140-2, and NUCu-140-3 Steels Solutionized at 900 °C and Aged at Either 550 °C or 500 °C**

| | Aged 2 h at 550 °C | | | Aged 6 h at 500 °C | | |
|---|---|---|---|---|---|---|
| | Yield Stress (MPa) | UTS (MPa) | Elongation-to-Failure (Pct) | Yield Stress (MPa) | UTS (MPa) | Elongation-to-Failure (Pct) |
| NUCu-140-1 | 973 | 994 | 22 | 1001 | 1042 | 22 |
| NUCu-140-2 | 1049 | 1049 | 20 | — | — | — |
| NUCu-140-3 | 849 | 890 | 23 | 911 | 952 | 22 |

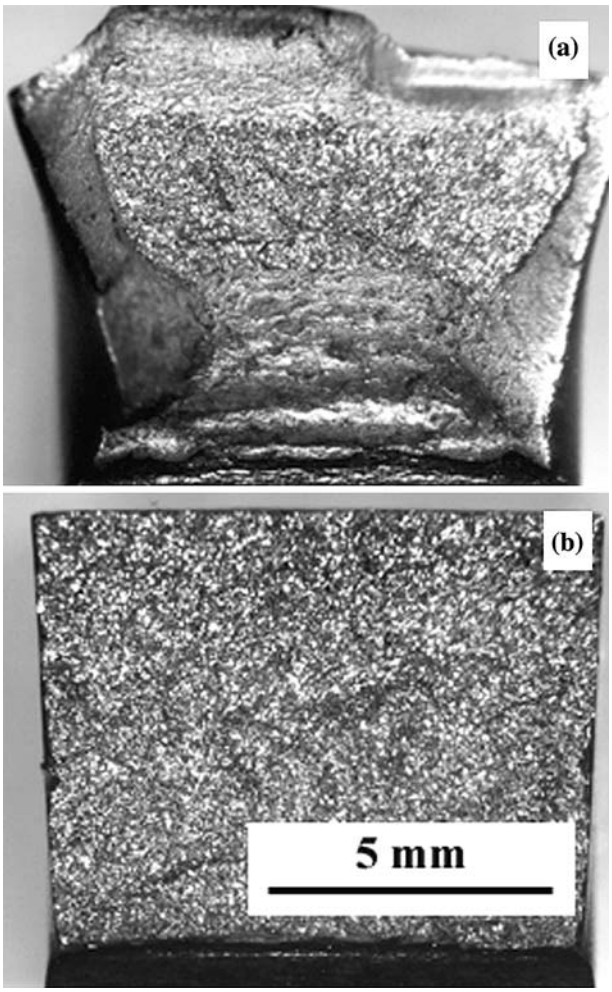


Fig. 4—The Charpy V-notch specimen fracture surfaces as observed by optical microscopy, for testing at room temperature: (*a*) NUCu-140-1 and (*b*) NUCu-140-2.

### C. *Welding Studies*

The microhardness profile and optical micrographs of the weld, FZ, HAZ, and base plate are presented in Figure 5. The Vickers microhardness value of the base plate (Figure 5(d)) is 3.2 GPa prior to welding. The microhardness in the HAZ (Figure 5(c)) is reduced to 2.0 GPa, whereas the FZ (Figure 5(b)) and weld (Figure 5(a)) have a microhardness value of approximately 2.7 GPa. The micrographs indicate that the grain size is much larger in the weld and FZ than in the HAZ or base metal. The grain size in the HAZ is equal to 3.2 $\mu$m, whereas the grain sizes in the FZ and weld are 15 and 34 $\mu$m, respectively. The grains within the FZ are either acicular in appearance or possess a blocklike appearance, whereas the grains within the weld have predominantly large blocklike shapes The grains in the HAZ are similar in appearance to the base metal, which consists of equiaxed grains with a smaller volume fraction of elongated grains.

### D. *Atom-Probe Tomography*

Figure 6(a) displays the atom-by-atom reconstruction of a $44 \times 44 \times 78$ nm$^3$ volume of NUCu-140-1 quenched from 900 °C and aged at 500 °C for 24 hours. The Cu atoms, shown as red dots, have aggregated to form Cu-rich precipitates, a few of which are labeled by arrows with the letter "A" in the figure. The mean radius, $\langle R \rangle$, of these precipitates, after 24 hours of aging, is 1.5 ± 0.1 nm and their number density is $N_V = (1.2 \pm 0.1) \times 10^{24}$ m$^{-3}$. Figure 7 displays the evolution of the quantity $\langle R \rangle$ with time when the steel is aged at 500 °C. The aging times investigated coincide with underaged, near peak hardness, and overaged conditions. The value of $\langle R \rangle$ increases from 0.9 nm at 3 hours to 1.8 nm at 100 hours, with the quantity $N_V$ concomitantly decreasing from $(3.3 \pm 0.7) \times 10^{24}$ to $(6.1 \pm 1.5) \times 10^{23}$ m$^{-3}$. The temporal evolution of the particle size distributions (PSDs) for all three aging times is discussed elsewhere in detail.[30] The compositional evolution of the Cu-rich precipitates is also presented in Reference 30, and the results are summarized briefly herein. Most importantly, the precipitates are Cu-rich containing significant concentrations of Fe, Ni, Al, and Mn. The precipitate cores contain only about 50 at. pct Cu after 3 hours of aging at 500 °C, and the core Cu concentration does not increase further with aging up to 100 hours. The precipitate contains a substantial amount of Fe. The precipitates are enriched to about 10 at. pct Ni, 15 at. pct Al, and 1.5 at. pct Mn after 24 hours of aging. At this time, a spherical shell surrounds each precipitate with increasing Ni, Al, and Mn concentrations developing at the precipitate/α-Fe matrix heterophase interfaces of the Cu-rich precipitates. Additionally, the gradient of the copper concentration profiles across the interfaces become sharper. After 100 hours of aging, the surrounding spherical shell contains 17 at. pct Ni, 15 at. pct Al, and 2.6 at. pct Mn, and these elements are concurrently depleted in the core of the Cu-rich precipitates. The enrichment of Ni, Al, and Mn at the precipitate/α-Fe matrix heterophase interfaces occurs subsequent to the formation of the Cu-rich precipitates, as discussed in detail elsewhere.[30]

In addition to the Cu-rich precipitates, a small NbC precipitate is observed, as shown in Figure 6(b), the more highly magnified area with the label "B" in Figure 6(a). This NbC precipitate shown is approximately 3.5 nm in radius and $N_V$ is estimated to be in the range $10^{21}$ to $10^{22}$ m$^{-3}$, which is two orders of magnitude less than the $N_V$ value for the Cu-rich precipitates.

Figure 8 displays a three-dimensional reconstruction of a sample region intersecting a grain boundary (GB), obtained from the NUCu-140 arc-melted heat after 100 hours of aging at 500 °C. The location of the GB is indicated by the dashed lines with the label "GB" in Figure 8 and is unambiguously identified by the discontinuity in a set of resolved {110} lattice planes visible in a different projection of the three-dimensional dataset. This GB is enriched in carbon with peak concentrations of up to approximately 3 at. pct locally, and additionally shows segregation of *B* and *P*, but no significant enrichment in *S*, as discussed elsewhere.[30] At the positions with label "A" are Cu-rich precipitates analogous to the Cu-rich precipitates visible in Figure 6. At label "B" in Figure 8 is a precipitate about 3 nm in radius that is highly enriched in Ni and Al. A proxigram

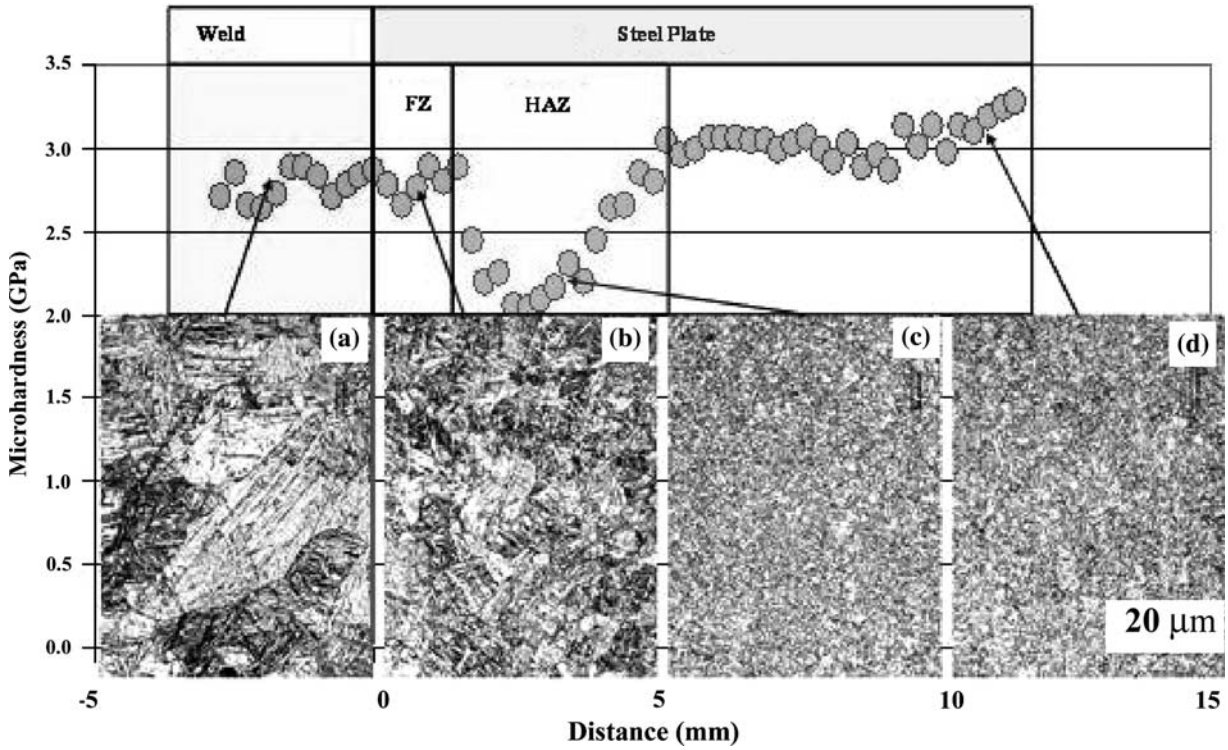


Fig. 5—Vickers microhardness profile and microstructures of the welded NUCu-140-1 steel plate. The microstructures are (*a*) weld, (*b*) fusion zone, (*c*) heat-affected zone, and (*d*) plate.

concentration profile analysis reveals that the composition of this precipitate is 36 ± 2 Ni – 40 ± 2 Al – 11 ± 2 Fe – 7 ± 1 Mn – 4 ± 1 Cu – 0.8 ± 0.4 Si (at. pct), whereas C and Nb were not detected.

## V. DISCUSSION

### A. *Microstructure and Mechanical Properties*

The multiple hardening peaks seen in Figure 2 are probably related to the temporal evolution of the complex Cu-rich precipitates.

The smaller CVN absorbed impact-energy values for NUCu-140-2 require discussion. Elevated concentration of *P* in this heat may play a role because segregation of *P* to GBs is known to result in embrittlement of steels.[42–44] Segregation of *P*, in addition to *C*, *B*, and *S*, is observed at a GB in a steel designated NUCu-170, which was made at the same time as NUCu-140-2.[30] However, the small differences in the *P* contents in the three heats (Table I) seem to be too small to give such a drastic reduction in Charpy value. Also, the cleavage nature of the fracture surface indicates that the fracture is mainly planar in nature and not intergranular. The grains of NUCu-140-2, when solutionized at 900 °C, are larger (10.3 $\mu$m compared with NUCu-140-1 and NUCu-140-3, 7.0, and 8.6 $\mu$m, respectively). Also, the grains in NUCu-140-2 are more acicular. The origin of the impact loading embrittlement in NUCu-140-2 requires further investigation.

The smaller yield strength value of NUCu-140-3, when compared with NUCu-140-1, is primarily attributed to the larger grain size, but the smaller Cu concentration, 1.29 wt pct, compared with 1.34 wt pct, plays a small role. The Hall–Petch relationship,[45,46] $\sigma_{YS} \propto d^{-1/2}$, where $d$ is the grain diameter and $\sigma_{YS}$ correlates with the reduced yield strength.

We attribute the change in yield strength and elongation-to-failure when varying the solutionizing temperature to the increase in volume fraction of large grains containing lathlike features, most likely indicating an increasing amount of low-carbon concentration martensite (Figure 1). The observed change in microstructure is related to the dissolution of NbC precipitates at the two higher solutionizing temperatures. Niobium-carbide precipitates pin the austenite GBs inhibiting grain growth during solutionizing.[47] At higher solutionizing temperatures, the NbC precipitates dissolve, leading to larger austenitic grain diameters, which increase the hardenability. Aging at 500 °C gives a larger value of yield strength than aging at 550 °C. This is attributed to a smaller solid solubility of Cu at the lower temperature.

We attribute the relatively high CVN absorbed impact energies measured at temperatures below 0 °C to a possible reduction of the local Peierls stress in the matrix. Small, misfitting precipitates may locally decrease the Peierls stress and reduce the rate of increase in yield strength on cooling,[48,49] possibly resulting in an improvement to the CVN absorbed impact-energy values at low temperatures.

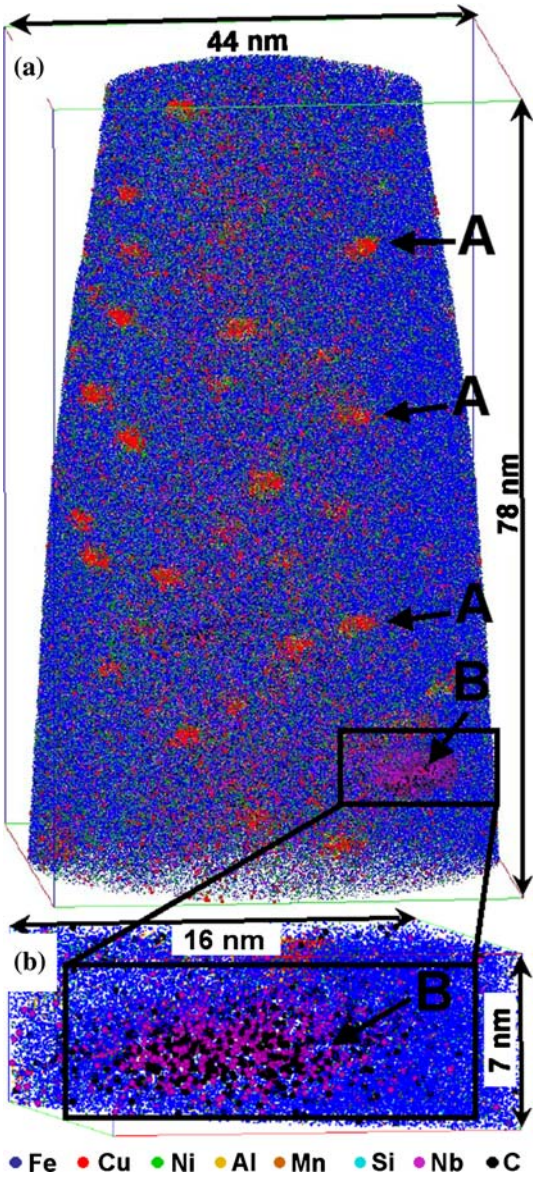


Fig. 6—Three-dimensional atom-by-atom LEAP tomographic reconstruction of NUCu-140-1 steel after quenching from 900 °C and aging at 500 °C for 24 h. Copper atoms are shown as red dots; see color legend at the bottom. Nanometer-sized Cu-rich precipitates have formed, see arrows with label "A" in (*a*), with an average radius of 1.5 ± 0.1 nm, at a number density of $N_V = (1.2 \pm 0.1) \times 10^{24}$ m$^{-3}$. Additionally, NbC precipitates are detected at a number density of approximately $10^{21}$ to $10^{22}$ m$^{-3}$; see magnified area "B" in (*b*). The dimensions of the reconstructed volume in (a) are 44 nm × 44 nm × 78 nm. Only 50 pct of the Fe atoms (blue color) are shown for clarity.

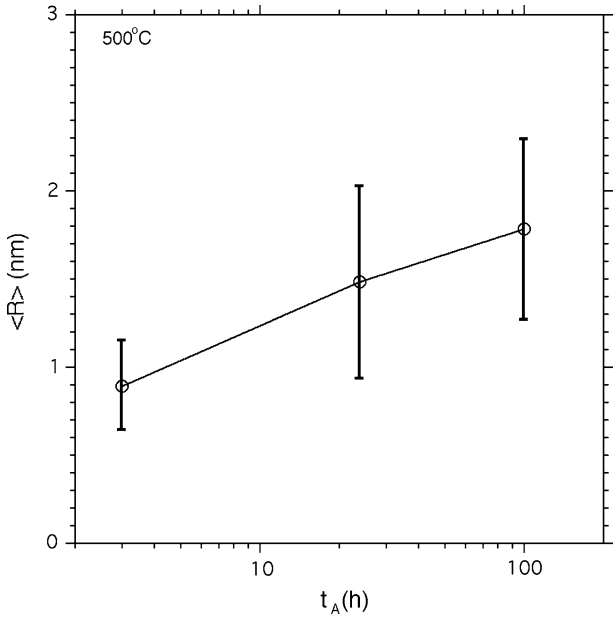


Fig. 7—Temporal evolution of the mean precipitate radius, ⟨*R*⟩, of the Cu-rich precipitates in NUCu-140-1 at 500 °C. The quantity ⟨*R*⟩ is given for 3, 24, and 100 h aging and was determined from PSDs containing 208, 94, and 42 precipitates, respectively.[30] The quantity ⟨*R*⟩ increases from 0.9 nm after 3 h aging to 1.8 nm after 100 h aging.

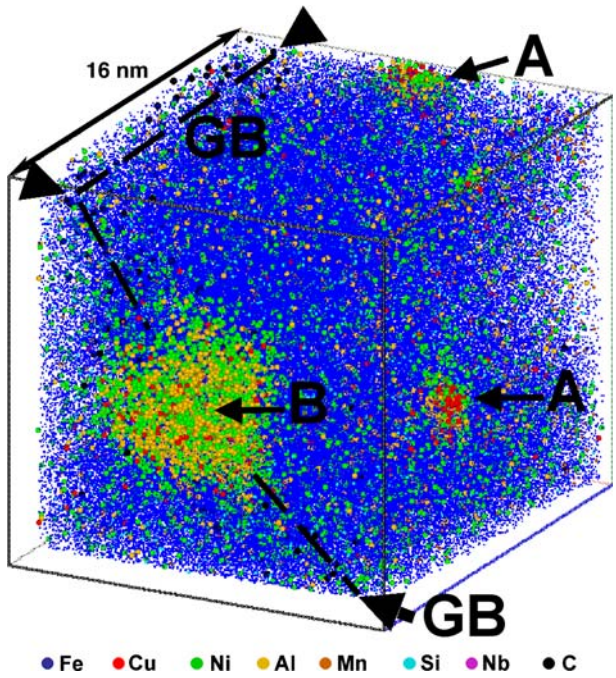


Fig. 8—Three-dimensional atom-by-atom conventional 3DAP tomographic reconstruction of NUCu-140-laboratory heat after quenching from 900 °C and aging 100 h at 500 °C. In addition to small nanometer-sized Cu-rich precipitates, label "A," a grain boundary that is enriched in *C*, *B*, and *P* runs diagonally through the reconstruction volume. A larger precipitate highly enriched in Ni and Al, label "B," has formed at the grain boundary. The dimensions of the reconstructed volume are 16 nm × 16 nm × 19 nm.

## B. *Welding*

The preliminary welding experiment indicates that a high-strength welding filler metal could be developed on the basis of this steel. The reduction in hardness values within the HAZ is most likely a consequence of the growth and coarsening of the Cu-rich precipitates since the matrix remains fine-grained ferrite as in the base plate. We note, however, that a brittle martensitic HAZ is *not* formed.

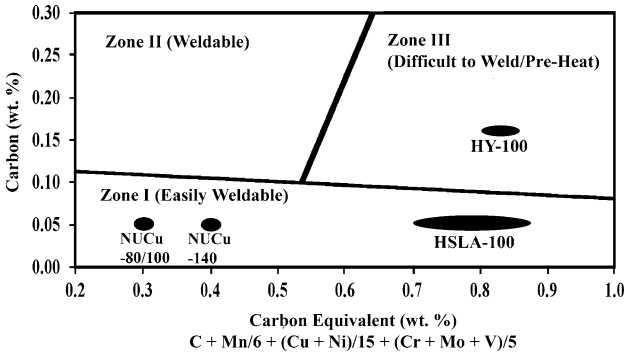


Fig. 9—Carbon equivalent diagram (Graville diagram) comparing the weldability of the NUCu series of steels with HSLA-100 and HY-100 steels. The comparatively low carbon equivalent of NUCu-140-*x*, 0.4 wt pct, indicates that the steels are weldable without concern for a brittle HAZ.

The carbon equivalent[7] of the NUCu-140 steels is determined by

$$\text{Carbon equivalent (wt pct)} = \text{C} + \left(\frac{\text{Mn}}{6}\right) + \left(\frac{\text{Cu} + \text{Ni}}{15}\right) + \left(\frac{\text{Cr} + \text{Mo} + \text{V}}{5}\right) \quad [2]$$

where "Carbon equivalent" indicates the susceptibility of the steel to cracking during welding. A value equal to 0.4 wt pct is obtained for the NUCu-140 steels, which as seen in a Graville diagram (Figure 9), resides in zone I, indicating that the steels are weldable without concern for a brittle HAZ. The value for carbon equivalent is greater than the 0.3 wt pct obtained for NUCu-100 but smaller than the values reported for HSLA-100 and HY-100 in Reference 2. In addition to the excellent weldability and lack of a HAZ, the steel does not contain Cr, leading to formation of $Cr^{6+}$, a carcinogenic fume, during welding.

### C. *Atom-Probe Tomography*

The nano-size Cu-rich precipitates, because of their comparatively large $N_V$ values, are responsible for the increase in strength during aging (Figure 2). The source of the strengthening from small coherent Cu-rich precipitates in steels, however, is unresolved and has been recently reviewed.[50] The source of this controversy is possibly a result of a combination of a number of precipitation strengthening mechanisms include lattice mismatch, modulus mismatch, and chemical hardening.[51–57] Also, when the dislocation enters the precipitate two partial dislocations are created that combine when the dislocation leaves the precipitate. Energy must be supplied to move the dislocation out of the precipitate.

The Fe content in the Cu-rich precipitates, as measured in this investigation, is about 25 at. pct.[30] Previous atom-probe studies of thermally aged Fe-Cu–based alloys have consistently detected significant amounts of Fe in Cu-rich precipitates about 2 nm in radius, in both binary Fe-Cu alloys[20,58] and multicomponent Fe-Cu–based alloys.[27,28,30,59] Small-angle neutron scattering (SANS),[56,60] using indirect methods that involve magnetic scattering for deconvoluting the precipitate composition, however, suggests a much smaller amount of Fe of up to 10 at. pct in the precipitates. We note that SANS provides precipitate compositions based on questionable assumptions,[61] whereas the APT results are model independent. Additionally, the recent first-principles calculations by Liu *et al.*[55] finds that the shear modulus relevant for dislocation glide varies at absolute 0 K from a negative value of 20 GPa for pure bcc Cu to a positive value of 78 GPa for bcc Fe, with a zero value for compositions near 50 at. pct Fe and 50 at. pct Cu. The results of this study predict that bcc Cu precipitates with Cu-rich concentrations, in a binary Fe-Cu alloy, are mechanically unstable, which is consistent with APT observations showing significant quantities of Fe in Cu precipitates with about 2-nm radius.[20,27,28,30,58,59]

Nickel and Mn spherical shell enrichment has been observed for model Fe-Cu-Ni and Fe-Cu-Ni-Mn steels,[30,58,59,62–64] but the concomitant enrichment in Al is a new result. Approximately equal proportions of Ni and Al in the spherical shell surrounding the Cu-rich core at 100 hours of aging may possibly be related to formation of a B2 ordered intermetallic phase. This conclusion cannot be made on stoichiometry alone. Conventional XRD studies have proven inconclusive because of counting statistics limitations. Recent synchrotron radiation experiments on the similar NUCu-170 steel at the Advanced Photon Source (APS), Argonne National Laboratory, however, has successfully identified the Ni-Al-Mn enrichment as a B2 crystalline structure.[65] The segregation of Ni, Al, and Mn to the precipitate/α-Fe matrix heterophase interfaces may possibly slow growth and coarsening, which makes the steel less prone to weakening resulting from overaging of the precipitates.

The presence of a larger, 3-nm radius, precipitate heterogeneously nucleated at a GB consisting predominantly of equal quantities of Ni and Al indicates that precipitates of this stoichiometry are stable within this steel at this temperature. The composition of the precipitate is suggestive of a NiAl (B2 structure) precipitate with Fe, Mn, and Cu substituting for Ni and Al in presently unknown proportions. The presence of NiAl precipitates at a GB and Ni-Al-Mn enrichments at the heterophase interface of the Cu-rich precipitates indicates that the driving force for homogeneous nucleation is not sufficient, at the given composition and thermal treatment, to obtain NiAl (B2) precipitates within the ferrite grains.

## VI. SUMMARY AND CONCLUSIONS

The details on the investigation of an essentially ferritic nanoscale precipitation-strengthened steel, NUCu-140 (140 designates the nominal yield stress in ksi), are presented. The steel is derived from the United

States Navy's current HSLA-100 steel by increasing the Cu, Ni, and Al concentrations and omitting Cr and Mo.

1. The steel achieves a 965 MPa yield strength, elongation-to-failure values greater than 15 pct, and good CVN absorbed impact-energy values as high as 74 J at −40 °C by simple heat treatment of solutionizing (austenitizing) at 900 °C, followed by a quench into water at room temperature, and subsequent aging for 2 hours at 550 °C.
2. The increase in strength is derived from a large number density (approximately $10^{23}$ to $10^{24}$ $nm^{-3}$) of Cu-rich coherent precipitates containing Fe, Ni, Al, and Mn.
3. Segregation of Ni, Al, and Mn to the precipitate/$\alpha$-Fe matrix heterophase interfaces of the Cu-rich precipitates is observed at 24 hours of aging. This segregation becomes more distinct with further aging to 100 hours.
4. Heterogeneous nucleation of a larger, 3-nm radius, precipitate within a grain boundary is observed. The stoichiometry of the precipitate is suggestive of a NiAl (B2 structure) precipitate with Fe, Mn, and Cu substituting for Ni and Al in presently unknown proportions.
5. The HAZ formed within NUCu-140 steel plate during welding is ductile. The microstructure in the plate's HAZ is ferritic after welding. The hardness in the HAZ is reduced, however, because of possible overaging of the Cu-rich precipitates. The steel's carbon equivalent, 0.4 wt pct, indicates that the steel may be weldable without preheat or postheat.

## ACKNOWLEDGMENTS

This research is supported by the Office of Naval Research (Grant No. N00014-03-1-0252), Dr. Julie Christodoulou, grant officer. Atom-probe tomographic analyses were performed at the Northwestern University Center for Atom-Probe Tomography (NUCAPT), and the LEAP tomograph was purchased with funding from the NSF-MRI (Grant No. DMR-0420532, Dr. Charles Bouldin, monitor) and ONR-DURIP (Grant No. N00014-0400798, Dr. Julie Christodoulou, monitor) programs. Additionally, the LEAP tomograph was enhanced in late April 2006 with a picosecond laser with funding from ONR-DURIP (Grant No. N0014-06-1-0539). This work made use of Central Facilities supported by the MRSEC program of the National Science Foundation (Grant No. DMR-0520513) at the Materials Research Center of Northwestern University.

## REFERENCES

1. A.P. Coldren and T.B. Cox: *Laboratory DTR*, 1986.
2. E.J. Czyrycka, R.E. Link, R.J. Wong, D.A. Aylor, T.W. Montemarano, and J.P. Gudas: *Nav. Eng. J.*, 1990, vol. 102, p. 63.
3. S.K. Dhua, D. Mukerjee, and D.S. Sarma: *Metall. Mater. Trans. A*, 2001, vol. 32A, p. 2259.
4. S.K. Dhua, A. Ray, and D.S. Sarma: *Mater. Sci. Eng. A*, 2001, vol. 318, p. 197.
5. T.W. Montemarano, B.P. Sack, J.P. Gudas, M.G. Vassilaros, and H.H. Vanderveldt: *J. Ship Prod.*, 1986, vol. 2, p. 145.
6. A.K. Sinha: *Physical Metallurgy Handbook*, McGraw-Hill, New York, NY, 2003.
7. R.W.K. Honeycombe and H.K.D.H. Bhadeshia: *Steels Microstructure and Properties*, Arnold, London, 1996.
8. R.P. Foley and M.E. Fine: in *Int. Conf. on Processing, Microstructure and Properties of Microalloyed and Other Modern High Strength Low Alloy Steels*, A.J. DeArdo, ed., ISS and TMS, Pittsburgh, PA, 1991, p. 315.
9. R.P. Foley: Ph.D. Thesis, Northwestern University, Evanston, IL, 1992.
10. C.S. Smith and E.W. Palmer: *Trans. AIME*, 1933, vol. 105, p. 133.
11. C.H. Lorig: *Metal Progr.*, 1935, vol. 27, p. 53.
12. C.H. Lorig and R.R. Adam: *Copper as an Alloying Element in Steel and Cast Iron*, McGraw-Hill, New York, NY, 1948.
13. J.L. Gregg and B.N. Daniloff: *The Alloys of Iron and Copper*, McGraw-Hill, New York, NY, 1934.
14. M.E. Fine, R. Ramanathan, S. Vaynman, and S.P. Bhat: in *Int. Symp. on Low-Carbon Steels for the 90's*, R.I. Asfahani and G. Tither, eds., TMS, Pittsburgh, PA, 1993, p. 511.
15. S. Vaynman and M.E. Fine: in *Int. Symp. on Steel for Fabricated Structures*, R.I. Asfahani and R.L. Bodnar, eds., AISI and ASM International, Cincinnati, OH, 1999, p. 59.
16. S. Vaynman, M.E. Fine, G. Ghosh, and S.P. Bhat: in *Materials for The New Millennium*, K.P. Chong, ed., ASCE, Washington, DC, 1996, vol. 2, p. 1551.
17. S. Vaynman, R.S. Guico, M.E. Fine, and S.J. Manganello: *Metall. Mater. Trans. A*, 1997, vol. 28A, p. 1274.
18. S. Vaynman, M.E. Fine, R.I. Asfahani, D.M. Bormet, and C. Hahin: in *Microalloyed Steel*, R.I. Asfahani, R.L. Bodnar and M.J. Merwin, eds., ASM, Columbus, OH, 2002.
19. S.R. Goodman, S.S. Brenner, and J.R. Low Jr.: *Metall. Trans.*, 1973, vol. 4, p. 2363.
20. S.R. Goodman, S.S. Brenner, and J.R. Low Jr.: *Metall. Trans.*, 1973, vol. 4, p. 2371.
21. M.S. Gagliano: *Co-Precipitation of Copper and Niobium Carbide in a Low Carbon Steel*, Northwestern University, Evanston, IL, 2002, p. 239.
22. M.S. Gagliano and M.E. Fine: *Calphad*, 2001, vol. 25, p. 207.
23. M.S. Gagliano and M.E. Fine: *Metall. Mater. Trans. A*, 2004, vol. 35A, p. 2323.
24. M.K. Miller: *Atom Probe Tomography*, Kluwer Academic/Plenum Publishers, New York, NY, 2000.
25. T.F. Kelly and M.K. Miller: *Rev. Sci. Instrum.*, 2007, vol. 78, p. 031101.
26. D.N. Seidman: *Annu. Rev. Mater. Res.*, 2007, vol. 37, p. 127.
27. D. Isheim and D.N. Seidman: *Surf. Interface Anal.*, 2004, vol. 36, p. 569.
28. D. Isheim, M.S. Gagliano, M.E. Fine, and D.N. Seidman: *Acta Mater.*, 2006, vol. 54, p. 841.
29. S. Vaynman, M.E. Fine, S. Lee, and H.D. Espinosa: *Scripta Mater.*, 2006, vol. 55, p. 351.
30. D. Isheim, R.P. Kolli, M.E. Fine, and D.N. Seidman: *Scripta Mater.*, 2006, vol. 55, p. 35.
31. T. Watanabe: *Tetsu-to-Hagané*, 1975, vol. 61, p. 2456.
32. R.A. Fournelle, E.A. Grey, and M.E. Fine: *Metall. Trans. A*, 1976, vol. 7A, p. 669.
33. C. Asada and T. Watanabe: *Trans. JIM*, 1968, vol. 9, suppl., p. 387.
34. S.C. Kolesar: *Precipitation Processes in Fe-Base, Ferritic, Ni-Al Alloys*, Northwestern University, Evanston, IL, 1971.
35. H.A. Calderon: *Development of BCC Fe Base Alloys with Coherent Precipitates*, Northwestern University, Evanston, IL, 1983.
36. T.T. Tsong: *Atom-Probe Field Ion Microscopy*, Cambridge University Press, Cambridge, United Kingdom, 1990.
37. O.C. Hellman, J.A. Vandenbroucke, J. Blatz du Rivage, and D.N. Seidman: *Mater. Sci. Eng. A*, 2002, vol. 327, p. 29.
38. O.C. Hellman, J. Blatz du Rivage, and D.N. Seidman: *Ultramicrosc.*, 2003, vol. 95, p. 199.
39. O.C. Hellman and D.N. Seidman: *Mater. Sci. Eng. A*, 2002, vol. 327, p. 24.
40. R.P. Kolli and D.N. Seidman: *Microsc. Microanal.*, 2007, vol. 13, p. 272.

41. M.K. Miller and E.A. Kenik: *Microsc. Microanal.*, 2004, vol. 10, p. 336.
42. C.J. McMahon Jr.: *Interface Sci.*, 2004, vol. 12, p. 141.
43. D.F. Stein and L.A. Heldt: in *Interfacial Segregation*, W.C. Johnson and J.M. Blakely, eds., ASM, Metals Park, OH, 1979.
44. M. Guttman and D. McLean: in *Interfacial Segregation*, W.C. Johnson and J.M. Blakely, eds., ASM, Metals Park, OH, 1979.
45. E.O. Hall: *P. Phys. Soc., Ser. B*, 1951, vol. 64, p. 747.
46. N.J. Petch: *J. Iron Steel Inst.*, 1954, vol. 173, p. 25.
47. A.J. DeArdo: *Int. Mater. Rev.*, 2003, vol. 48, p. 371.
48. A. Urakami and M.E. Fine: *Scripta Mater.*, 1970, vol. 4, p. 667.
49. M.E. Fine, A. Tongen, and M.S. Gagliano: in *Electron Microscopy: Its Role in Materials Research, The Mike Meshii Symp.*, J.R. Weertman, M.E. Fine, K. Faber, W. King, and P. Liaw, eds., TMS, San Diego, CA, 2003, p. 229.
50. M.E. Fine and D. Isheim: *Scripta Mater.*, 2005, vol. 53, p. 115.
51. K.F. Russell and L.M. Brown: *Acta Metall.*, 1972, vol. 20, p. 969.
52. E. Nembach: *Particle Strengthening of Metals and Alloys*, Wiley-Interscience, New York, NY, 1997.
53. T. Harry and D.J. Bacon: *Acta Mater.*, 2002, vol. 50, p. 209.
54. S. Lozano-Perez, M.L. Jenkins, and J.M. Titchmarsh: *Philos. Mag. Lett.*, 2006, vol. 86, p. 367.
55. J.Z. Liu, A. van de Walle, and M.D. Asta: *Phys. Rev. B: Condens. Matter*, 2005, vol. 72, p. 144109.
56. K. Osamura, H. Okuda, M. Ochiai, M. Takashima, K. Asano, M. Furusaka, K. Kishida, and F. Kurosawa: *ISIJ Int.*, 1994, vol. 34, p. 359.
57. A. Deschamps, M. Militzer, and W.J. Poole: *ISIJ Int.*, 2001, vol. 41, p. 196.
58. G.M. Worrall, J.T. Buswell, C.A. English, M.G. Hetherington, and G.D.W. Smith: *J. Nucl. Mater.*, 1987, vol. 148, p. 107.
59. P.J. Pareige, K.F. Russell, and M.K. Miller: *Appl. Surf. Sci.*, 1996, vols. 94–95, p. 362.
60. R. Kampmann and R. Wagner: in *Atomic Transport and Defects in Metals by Neutron Scattering*, C. Janot, W. Petry, D. Richter, and T. Springer, eds., Springer-Verlag, Berlin, 1986, p. 73.
61. M.E. Fine, J.Z. Liu, and M.D. Asta: *Mater. Sci. Eng. A*, 2007, vol. 463, p. 271.
62. K. Osamura, H. Okuda, K. Asano, M. Furusaka, K. Kishida, F. Kurosawa, and R. Uemori: *ISIJ Int.*, 1994, vol. 34, p. 346.
63. T. Koyama and H. Onodera: *Mater. Trans.*, 2005, vol. 46, p. 1187.
64. T. Koyama, K. Hashimoto, and H. Onodera: *Mater. Trans.*, 2006, vol. 47, p. 2765.
65. R.P. Kolli, Z. Mao, D.T. Keane, and D.N. Seidman: *Appl. Phys. Lett.*, 2007, vol. 91, p. 241903.